CrossMark

Numerical study of mixed convection heat transfer inside a vertical microchannel with two-phase approach

Mohammad Reza Tavakoli[1] · Omid Ali Akbari[1] · Anoushiravan Mohammadian[1] · Erfan Khodabandeh[1] · Farzad Pourfattah[1]

Abstract

The current study investigates the laminar and two-phase nanofluid flow inside a two-dimensional rectangular microchannel with the ratio of length to height of $L/H = 120$. This study is simulated by using finite volume method in two-dimensional coordinates. Because most of the miniature equipments are affected by the oscillating heat flux, we try to study the hydrodynamical behavior of flow and heat transfer with oscillating heat flux boundary condition. The present research has been carried out in Reynolds numbers of 150–1000 and Ag nanoparticles volume fractions of 0–4% by applying slip and no-slip boundary conditions. Also, in order to estimate the heat transfer behavior and the computational fluid dynamics, two-phase mixture method is employed. The obtained results are analyzed and presented as the contours of Nusselt number, friction coefficient, pressure drop, thermal resistance and temperature. The results also revealed that, applying slip boundary condition on microchannel walls and the enhancement of fluid velocity, Grashof number and volume fraction of nanoparticles cause the improvement of Nusselt number, reduction of thermal resistance and total entropy generation and the augmentation of pressure drop. According to the obtained results, the presence of oscillating heat flux affects the changes of Nusselt number, significantly. In comparison with the pure water fluid with Reynolds numbers of 1000, 700 and 400, in Grashof number of 1000 with no-slip boundary condition on microchannel walls, the enhancement of average Nusselt number in volume fraction of 4% in the same Reynolds numbers is 45%. Also, in mentioned conditions, the pressure drop increases almost 2.8 times further.

List of symbols

A	Area (m^2)
$B = \beta/H$	Dimensionless slip velocity
C_f	Skin friction factor
C_p	Heat capacity (J kg^{-1} K^{-1})
H	Microchannel height (μm)
k	Thermal conductivity coefficient (W m^{-1} K^{-1})
L	Microchannel length (μm)
g	Gravity acceleration (m s^{-2})
Nu	Nusselt number
P	Fluid pressure (Pa)
s	Entropy (J kg^{-1} K^{-1})
$Pr = \upsilon_f/\alpha_f$	Prandtl number
$q''(X)$	Oscillating heat flux (W m^{-2})
q''_0	Constant heat flux (W m^{-2})
R	Thermal resistance (m K W^{-1})
$Re = \rho_m u_c d/\mu_m$	Reynolds number
T	Temperature (K)
$X = \frac{x}{H} = \bar{x},\ Y = \frac{y}{H} = \bar{y}$	Cartesian dimensionless coordinates
u, v	Velocity components in x, y directions (m s^{-1})
u_c	Inlet velocity in x directions (m s^{-1})
u_s	Brownian motion velocity (m s^{-1})
T	Silicon layer thickness (μm)

Greek symbols

β	Slip velocity coefficient (m)
φ	Nanoparticles volume fraction
μ	Dynamic viscosity (Pa s)

✉ Mohammad Reza Tavakoli
  mrtavak@cc.iut.ac.ir

[1] Department of Mechanical Engineering, Isfahan University of Technology, Isfahan 84156-83111, Iran

$\theta = (T - T_C)/\Delta T$	Dimensionless temperature
ρ	Density (kg m^{-3})
τ	Shear stress (N m^{-2})
υ	Kinematics viscosity (m^2 s^{-1})

Super- and subscripts

Ave	Average
c	Cold
Eff	Effective
f	Base fluid (pure water)
H	Hot
In	Inlet
Max	Maximum
Min	Minimum
nf	Nanofluid
Out	Outlet
S	Solid nanoparticles

Introduction

Today, due to the consumption of irreversible energy sources and the production of environmental prolusions, optimizing heat transfer process by using cooling fluids has become very important in the numerous industries such as energy generation industries, aerospace, petrochemicals, transportation, machining and electronic industries. In order to obtain high efficiency, the heat transfer equipment needs minimized dimensions and the enhancement of heat transfer in each unit of surface area. The development of technology in recent decades, the changes of rheological properties of cooling fluids and generating steady solid–liquid suspensions called nanofluid cause the optimization of thermal efficiency of industrial tools and heat exchangers. Hence, increasing heat transfer through nanofluids has been reported by many researchers [1–14]. In recent decades, for minimizing the dimensions of heat transfer equipment, producing channels with microdimensions as heat exchangers (microchannels) has been widely considered. Microchannel is an equipment used for controlling the temperature of electronic chips with high heat fluxes. Some advantages of microchannel are compressibility, high ratio of surface to volume, high heat transfer and thermal performance and lightweight. These advantages of microchannel along with novel heat transfer methods entail more heat transfer enhancement in the electronic industries. Therefore, numerous researchers have studied the nanofluid flow in micro- and macro-dimensions [15–31]. Nikkhah et al. [32] numerically investigated the laminar flow of water/functionalized multi-walled carbon nanotubes in a two-dimensional rectangular microchannel by applying oscillating heat flux and slip velocity boundary condition on walls. Their numerical results revealed that the increase in volume fraction, slip velocity coefficient and Reynolds number entail the enhancement of Nusselt number and heat transfer. Safaei et al. [33] numerically studied the laminar flow of water/Cu nanofluid in an inclined ribbed microchannel with the angles of 0°–90° and volume fractions of 0–4% of solid nanoparticles in Reynolds number of 50 and Richardson numbers of 0.1–10. They figured out that, in low Reynolds numbers, the gravity force has an important effect on heat transfer and fluid flow, and by increasing volume fraction of nanoparticles, the inclined angle of microchannel and Richardson number, heat transfer improves. Raisi et al. [34] numerically studied the laminar flow and heat transfer in a two-dimensional rectangular microchannel with constant thermal boundary condition and constant surface temperature with slip boundary condition on walls. Their results indicated that the existence of slip boundary condition on solid walls in low Reynolds numbers does not have any considerable effect on heat transfer enhancement and in higher Reynolds numbers causes significant enhancement of heat transfer. Elshazly et al. [35] investigated the convection heat transfer on the internal surface of vertical and inclined elliptical tubes placed in front of flow. In their research, the applied heat flux on the internal surface of tubes and the effect of inclined angle and flow direction on heat transfer coefficient have been investigated. They stated that, in constant Rayleigh number, by increasing the inclined angle and flow direction, the average Nusselt number enhances. Lotfi et al. [36] simulated the nanofluid flow in a horizontal tube by using three different methods of single-phase, two-phase mixture model and two-phase Euler model. By comparing their numerical results with the results of an experimental study, they found that two-phase mixture model is more accurate than other models. Behzadmehr et al. [37] numerically investigated the turbulent and developed nanofluid flow in different Reynolds numbers with volume fraction of 1% of Cu nanoparticles inside a circular tube. In this research, they used two-phase and single-phase models for investigating the fluid flow and heat transfer and indicated that two-phase mixture model has better coincidence with the experimental results. Akbari et al. [38] numerically studied the laminar and forced nanofluid flow in a two-dimensional ribbed microchannel and revealed that, by increasing the number of ribs, volume fraction of nanoparticles and Reynolds number, the rate of heat transfer enhances. On the other hand, the existence of rib on the direction of flow motion causes the creation of velocity gradients and the enhancement of contact surface and average friction coefficient. Behnampour et al. [39] investigated the effect of using different shapes of rib on laminar flow and heat transfer of water/Ag nanofluid with different volume fractions inside a

rectangular ribbed microchannel. They concluded that, in all Reynolds numbers, the optimization of heat transfer is not observed in the rectangular rib shape, and in high Reynolds numbers, using trapezoidal rib is not recommended.

In many industrial tools, the existence of timed fans causes the creation of oscillating thermal removal from these equipments. In the present numerical research, the mixed and laminar flow and heat transfer of nanofluid in a two-dimensional microchannel with oscillating heat flux boundary condition are numerically simulated using finite volume method in Cartesian coordinates. The results of the present research indicate the dependency of flow and heat transfer parameters such as Nusselt number, thermal resistance, pressure drop and friction coefficient with thermal boundary condition (oscillating heat flux) and hydrodynamical (slip and no-slip boundary conditions), volume force of gravity acceleration and volume fraction of nanoparticles. The advantage of this research is considering vertical microchannel and applying inconstant heat flux and slip boundary condition on microchannel walls in contact with fluid. Also, in order to simulate different phases of solid (nanoparticles) and liquid (base fluid) more accurately, two-phase mixture model is used.

Problem statement

In the current study, the mixed, laminar and two-phase flow and heat transfer of water/Ag nanofluid in vertical microchannel have been numerically simulated. The studied microchannel is rectangular and two dimensional. The length of microchannel is $L = 4.8$ mm, and its height is $H = 40$ μm. The wall of microchannel is made of silicon, and its thickness is $t = 15$ μm. The external wall of microchannel at the left side is insulated, and the right side wall is under the influence of oscillating heat flux with the function of $q''(X) = 2q_0'' + q_0'' \sin\left(\frac{\pi X}{4}\right)$. The inlet cooling fluid enters the channel with uniform velocity with the temperature of $T_c = 293$ K. This simulation has been carried out in volume fractions of 0, 2 and 4% of Ag nanoparticles and Reynolds numbers of 150, 400, 700 and 1000. Also, the effect of gravity domain on laminar flow and heat transfer behavior in Grashof numbers of 1000 and 10,000 is investigated. Figure 1 demonstrates the simulated geometry of the present study.

The present study has been carried out for no-slip ($B = 0$) and slip ($B = 0.1$) velocity boundary conditions on the internal walls of microchannel which are in contact with fluid. Also, the solid nanoparticles are uniform and spherical with the diameter of 10 nm. The suspension of pure water as the base fluid and nanoparticles in the studied
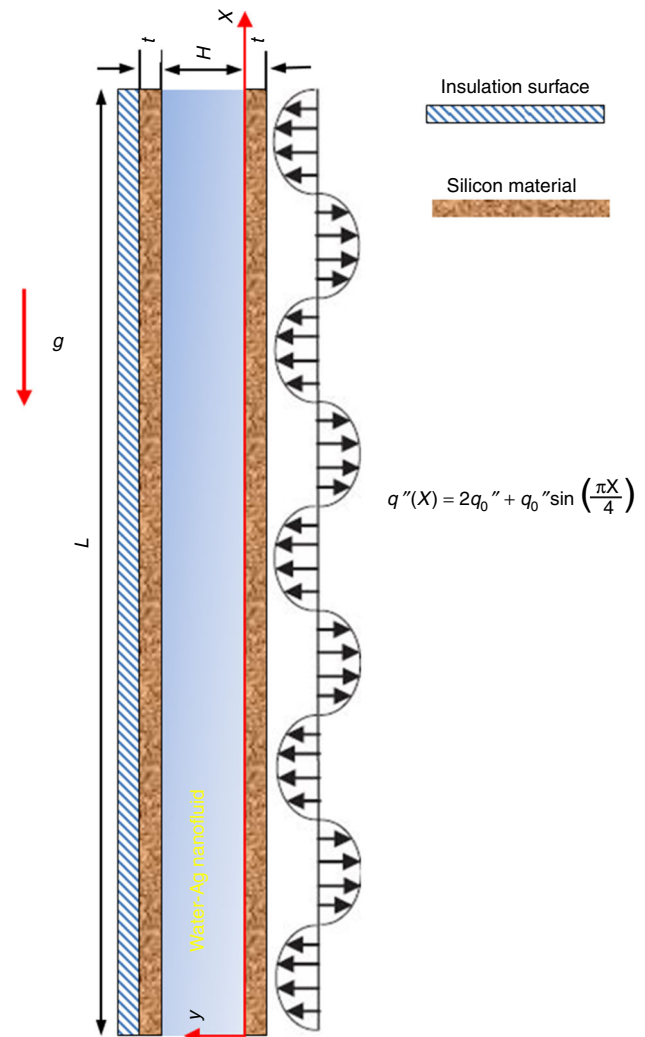

Fig. 1 Schematic of studied geometrics in the present research

volume fractions is simulated by two-phase mixture model as a Newtonian and steady fluid. The nanofluid properties are constant and independent from temperature. In Table 1, the properties of base fluid and Ag nanoparticles are presented [40].

Mathematical modeling

Governing equations and boundary conditions

The governing equations on laminar and two-phase nanofluid flow are continuity, momentum and energy equations [41–43]:

$$\nabla \cdot (\rho_m \vec{V}_m) = 0 \tag{1}$$

Table 1 Thermophysical properties of base fluid and solid nanoparticles [40]

Material	Pr	ρ/kg m^{-3}	C_p/J kg^{-1} K^{-1}	k/W mK^{-1}	μ (Pa S) $\times 10^{-6}$
Pure water	6.2	997	4179	0.613	891
Ag	–	10,500	235	429	–

$$\vec{V}_m = \frac{\sum_{Z=1}^{n} \varphi_Z \rho_Z \vec{V}_Z}{\rho_m} = V_Z \tag{2}$$

$$\rho_m = \sum_{Z=1}^{n} \varphi_Z \rho_Z \tag{3}$$

$$\nabla \cdot (\rho_m \vec{V}_m \vec{V}_m) = -\nabla P_m + \nabla \cdot \left[\mu_m \left(\nabla \vec{V}_m + \nabla \vec{V}_m^T \right) \right]$$
$$+ \nabla \cdot \left(\sum_{Z=1}^{n} \varphi_Z \rho_Z \vec{V}_{dr,Z} \vec{V}_{dr,Z} \right)$$
$$+ (\rho\beta)_m (T - T_c) \vec{g} \tag{4}$$

$$\vec{V}_{dr,Z} = \vec{V}_Z - \vec{V}_m \tag{5}$$

$$\mu_m = \sum_{Z=1}^{n} \varphi_Z \mu_Z = \varphi_{bf}\mu_{bf} + \varphi_{np}\mu_{np} \rightarrow \mu_{np}$$
$$= -0.188 + 537.42\varphi_{np} \tag{6}$$

$$\nabla \cdot (\rho_m h_m \vec{V}_m) + \nabla \cdot (P\vec{V}_m) = \nabla \cdot (k_m \nabla T) \tag{7}$$

$$\rho_m h_m = \sum_{Z=1}^{n} (\varphi_Z \rho_Z h_Z), \quad k_m = \sum_{Z=1}^{n} \varphi_Z(k_Z) \tag{8}$$

In the above equations, V_m is the average velocity of mixture, $V_{dr,z}$ is driving velocity for the secondary phase of z and the indexes of T, P, φ, μ and ρ are, respectively, the temperature, pressure, volume fraction, dynamic viscosity and density. In Eqs. (1–8), the indexes of z, dr and m are, respectively, the secondary phase of z, driving and the mixture (solid–liquid phases).

For non-dimensioning the parameters explained in results and discussion section, the following definitions are used [44],

$$X = \frac{x}{H} = \bar{x} \quad Y = \frac{y}{H} = \bar{y} \quad \bar{v} = \frac{v}{\alpha_f/H}$$
$$\theta = \frac{T - T_c}{\Delta T} \quad \bar{u} = \frac{u}{\alpha_f/H} \quad B = \frac{\beta}{H}$$
$$\Delta T = \frac{q_0'' H}{k_f} \quad Pr = \frac{v_f}{\alpha_f} \quad P = \frac{\overline{P}}{\rho_m(\alpha_f/H)^2} \tag{9}$$

The non-dimensional equations for two-phase and laminar flow are as follows:

Continuity equation [42]:

$$\frac{\partial \bar{u}_m}{\partial \bar{x}} + \frac{\partial \bar{v}_m}{\partial \bar{y}} = 0 \tag{10}$$

x-momentum equation:

$$\left[\bar{u}_m \frac{\partial \bar{u}_m}{\partial \bar{x}} + \bar{v}_m \frac{\partial \bar{v}_m}{\partial \bar{y}} \right] = -\frac{\partial \bar{p}}{\partial \bar{x}} + \frac{\rho_f}{\rho_m} \left[\frac{\partial}{\partial \bar{x}} \left(Pr \frac{\mu_m}{\mu_f} \frac{\partial \bar{u}_m}{\partial \bar{x}} \right) \right.$$
$$\left. + \frac{\partial}{\partial \bar{y}} \left(Pr \frac{\mu_m}{\mu_f} \frac{\partial \bar{u}_m}{\partial \bar{y}} \right) \right] + (1 - \varphi) \frac{\rho_f}{\rho_m}$$
$$\times \left[\bar{u}_{dr,f} \frac{\partial \bar{u}_{dr,f}}{\partial \bar{x}} + \bar{v}_{dr,f} \frac{\partial \bar{u}_{dr,f}}{\partial \bar{y}} \right] + \varphi \frac{\rho_p}{\rho_m} \left[\bar{u}_{dr,p} \frac{\partial \bar{u}_{dr,p}}{\partial \bar{x}} + \bar{v}_{dr,p} \frac{\partial \bar{u}_{dr,p}}{\partial \bar{y}} \right] \tag{11}$$

y-momentum equation:

$$\left[\bar{u}_m \frac{\partial \bar{v}_m}{\partial \bar{x}} + \bar{v}_m \frac{\partial \bar{v}_m}{\partial \bar{y}} \right] = -\frac{\partial \bar{p}}{\partial \bar{y}} + \frac{\rho_f}{\rho_m} \left[\frac{\partial}{\partial \bar{x}} \left(Pr \frac{\mu_m}{\mu_f} \frac{\partial \bar{v}_m}{\partial \bar{x}} \right) \right.$$
$$\left. + \frac{\partial}{\partial \bar{y}} \left(Pr \frac{\mu_m}{\mu_f} \frac{\partial \bar{v}_m}{\partial \bar{y}} \right) \right] + (1 - \varphi) \frac{\rho_f}{\rho_m} \left[\bar{u}_{dr,f} \frac{\partial \bar{v}_{dr,f}}{\partial \bar{x}} + \bar{v}_{dr,f} \frac{\partial \bar{v}_{dr,f}}{\partial \bar{y}} \right]$$
$$+ \varphi \frac{\rho_p}{\rho_m} \left[\bar{u}_{dr,p} \frac{\partial \bar{v}_{dr,p}}{\partial \bar{x}} + \bar{v}_{dr,p} \frac{\partial \bar{v}_{dr,p}}{\partial \bar{y}} \right] + \frac{(\beta\rho)_m}{(\beta\rho)_f} \frac{\rho_f}{\rho_m} RaPr\theta \tag{12}$$

Energy equation:

$$\frac{\rho_p C_{P_p}}{\rho_f C_{P_f}} \left[\bar{u}_p \frac{\partial}{\partial \bar{x}} (\varphi\theta) + \bar{v}_p \frac{\partial}{\partial \bar{y}} (\varphi\theta) \right]$$
$$+ \left[\bar{u}_f \frac{\partial}{\partial \bar{x}} ((1 - \varphi)\theta) + \bar{v}_f \frac{\partial}{\partial \bar{y}} ((1 - \varphi)\theta) \right]$$
$$= \frac{\partial}{\partial \bar{x}} \left(\frac{k_m}{k_f} \frac{\partial \theta}{\partial \bar{x}} \right) + \frac{\partial}{\partial \bar{y}} \left(\frac{k_m}{k_f} \frac{\partial \theta}{\partial \bar{y}} \right) \tag{13}$$

Volume fraction equation:

$$\frac{\partial(\varphi \bar{u}_m)}{\partial \bar{x}} + \frac{\partial(\varphi \bar{v}_m)}{\partial \bar{y}} + \frac{\partial(\varphi \bar{u}_{dr,p})}{\partial \bar{x}} + \frac{\partial(\varphi \bar{v}_{dr,p})}{\partial \bar{x}} = 0 \tag{14}$$

The thermal and hydrodynamical boundary conditions used in different sections of microchannel are as follows:

$$U = 1, \ V = 0 \text{ and } \theta = 0 \text{ for } X = 0 \text{ and } 0.375 \leq Y \leq 1.375 \tag{15}$$

$$V = 0 \text{ and } \frac{\partial \theta}{\partial X} = \frac{\partial U}{\partial X} = 0$$
$$\text{for } X = 120 \text{ and } 0.375 \leq Y \leq 1.375 \tag{16}$$

$$V = 0, \ U = 0 \text{ and } \frac{\partial \theta}{\partial Y} = 2q_0'' + q_0'' \sin\left(\frac{\pi X}{4}\right)$$
$$\text{for } Y = 0 \text{ and } 0 \leq X \leq 120 \tag{17}$$

$$V = 0, \ U_s = B \frac{\partial U}{\partial Y} \text{ and } k_{nf} \frac{\partial \theta}{\partial Y} = k_s \frac{\partial \theta}{\partial Y} \quad \text{for } Y$$
$$= 0.375 \text{ and } 0 \leq X \leq 120 \tag{18}$$

$$V = 0 \ , \ U = 0 \quad \text{and} \quad \frac{\partial \theta}{\partial Y} = 0 \quad \text{for } Y$$
$$= 1.75 \quad \text{and} \quad 0 \le X \le 120 \tag{19}$$

$$V = 0 \ , \ U_s = -B \frac{\partial U}{\partial Y} \quad \text{and} \quad k_{nf} \frac{\partial \theta}{\partial Y} = k_s \frac{\partial \theta}{\partial Y} \quad \text{for}$$
$$Y = 1.375 \quad \text{and} \quad 0 \le X \le 120 \tag{20}$$

The equations of thermophysical properties of nanofluid

Chon equation is used for calculating the thermal conductivity of nanofluid [45]. In Chon equation, the effects of fluid molecules and solid nanoparticles diameter, volume fraction of nanoparticles and fluid temperature are considered for calculating the thermal conductivity of nanofluid. This equation is considered for nanoparticle diameters of 11–150 nm.

$$\frac{k_{m}}{k_{f}} = 1 + 64.7 \, \phi^{0.746} \left(\frac{d_{f}}{d_{np}} \right)^{0.369} \left(\frac{k_{np}}{k_{f}} \right)^{0.7476} Pr^{0.9955} \, \text{Re}^{1.2321}$$
$$\text{Re} = \frac{\rho_{f} k_{b} T}{3\pi\mu^2 l_{f}}, \quad Pr = \frac{\mu_{f}}{\rho_{f} \alpha_{f}}, \quad \mu = A \times 10^{\frac{B}{T-C}}, \ C = 140 \, (\text{K}),$$
$$B = 247 \, (\text{K}), \quad A = 2.414 \times 10^{-5} \, (\text{Pa s}), \quad T = T_{in} \tag{21}$$

The dynamic viscosity is calculated by the following equation [46],

$$\mu_{\text{eff}} = \left(123\varphi^2 + 7.3\varphi + 1 \right) \mu_{f} \tag{22}$$

The specific heat capacity can be determined by the following equation [47],

$$\left(\rho \, c_{\text{p}} \right)_{\text{m}} = (1 - \varphi)(\rho \, c_{\text{p}})_{f} + \varphi(\rho \, c_{\text{p}})_{np} \tag{23}$$

Nanofluid density is calculated by the following equation [48],

$$\rho_{\text{m}} = \varphi \rho_{\text{np}} + (1 - \varphi)\rho_{f} \tag{24}$$

Thermal expansion coefficient is calculated by the following equation [49, 50],

$$\frac{\beta_{\text{eff}}}{\beta_{f}} = \left[\frac{1}{1 + \frac{(1-\varphi)\rho_{f}}{\varphi \, \rho_{\text{P}}}} \times \frac{\beta_{\text{P}}}{\beta_{f}} + \frac{1}{1 + \frac{\varphi \, \rho_{\text{P}}}{(1-\varphi)\rho_{f}}} \right] \tag{25}$$

Equations for calculating the output parameters

Friction coefficient is a parameter for investigating microchannel performance and can be calculated by the following equation,

$$Cf = \frac{2 \times \tau_{\text{w}}}{\rho u_{\text{in}}^2} \tag{26}$$

The average Nusselt number can be obtained as [51],

$$Nu_x = \frac{h \times H}{k_{f}} \quad \rightarrow \quad Nu_{\text{ave}} = \frac{1}{L} \int_0^L Nu_{\text{x}}(X) \, dX \tag{27}$$

The pressure drop in the inlet and outlet sections is defined as [52]:

$$\Delta P = P_{\text{in}} - P_{\text{out}} \tag{28}$$

The thermal resistance of hot wall of microchannel is calculated by the following equation [53],

$$R = \frac{T_{\max} - T_{\min}}{q_0'' \times A} = \frac{T_{\max} - T_{\text{in}}}{q_0'' \times A} \rightarrow A = W \times L \rightarrow R \times W$$
$$= \frac{T_{\max} - T_{\min}}{q_0'' \times L} \tag{29}$$

In Eq. (24), $T_{\max}$, $T_{\min}$, A and q_0'' are, respectively, the maximum temperature of bottom wall, the minimum temperature (temperature of inlet fluid), cross section of applied heat flux and the applied heat flux to the hot wall. The entropy generation caused by thermal irreversibility (heat transfer) equals with [54].

$$S_{gen} = \frac{k_{\text{eff}}}{\overline{T}^2} \left[\left(\frac{\partial \overline{T}}{\partial x} \right)^2 + \left(\frac{\partial \overline{T}}{\partial y} \right)^2 \right] \tag{30}$$

The entropy generation caused by flow irreversibility (friction coefficient) equals with [54],

$$S_{gen} = \frac{\mu_{\text{eff}}}{\overline{T}} \left\{ 2 \left[\left(\frac{\partial \overline{u}}{\partial x} \right)^2 + \left(\frac{\partial \overline{v}}{\partial y} \right)^2 \right] + \left(\frac{\partial \overline{u}}{\partial x} + \frac{\partial \overline{v}}{\partial y} \right)^2 \right\} \tag{31}$$

Total entropy generation including the entropy enhancement caused by heat transfer and flow friction is obtained as [55],

$$S_{gen} = \frac{k_{\text{eff}}}{\overline{T}^2} \left[\left(\frac{\partial \overline{T}}{\partial x} \right)^2 + \left(\frac{\partial \overline{T}}{\partial y} \right)^2 \right]$$
$$+ \frac{\mu_{\text{eff}}}{\overline{T}} \left\{ 2 \left[\left(\frac{\partial \overline{u}}{\partial x} \right)^2 + \left(\frac{\partial \overline{v}}{\partial y} \right)^2 \right] + \left(\frac{\partial \overline{u}}{\partial x} + \frac{\partial \overline{v}}{\partial y} \right)^2 \right\} \tag{32}$$

Numerical procedure

Assumptions and solving methods

In the current study, by using finite volume method, the mixed and laminar nanofluid flow is simulated as steady and Newtonian. Nanofluid properties are constant (homogeneous) and independent from temperature, and the behavior of two-phase nanofluid is determined by two-phase mixture model. On the right side wall of microchannel shown in Fig. 1, the sinusoidal heat flux is applied. In this research, the radiation effects are neglected. The second-order upwind discretization [56] and SIMPLEC algorithm [57] are employed for solving the governing equations. The maximum residual of present numerical procedure is considered 10^{-6}.

Mesh study and numerical solving procedure

In the current investigation, in order to ensure the results independency, the considered grid number has been changed to the regular and rectangular grids from 20,000 to 95,000. The studied parameters in the validation of the present study are Nusselt number along the hot wall and pressure drop differences in the inlet and outlet sections of microchannel. The changes of these two parameters are studied in Reynolds numbers of 150 and 700 for pure water fluid in no-slip boundary condition ($B = 0$) and Grashof number of 1000. According to Table 2, the grid number of 95,000 indicates more accurate results than other grid numbers. However, because the grid number of 70,000, comparing to the grid number of 95,000, has an acceptable error and needs less computational time, the grid number of 70,000 is used in the present numerical simulation. The gridding of present geometry with the selected grid number is shown in Fig. 2.

**Fig. 2** Regular grid structure on the part of the desired geometry
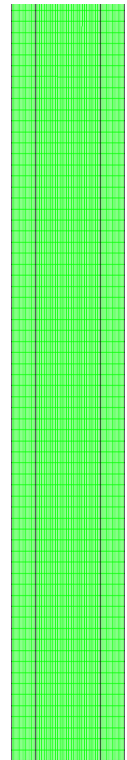
Validation

The results of the present study are validated with the numerical study of Safaei et al. [33] and the experimental study of Chein and Chuang [58]. Safaei et al. [33] numerically investigated the laminar flow and heat transfer of water/Cu nanofluid inside a two-dimensional microchannel with the angle of 90° (completely vertical channel) in Reynolds number of 50, 2% nanoparticles volume fraction and Richardson number of 10 (Fig. 3a). Also, Chein and Chuang [58] studied the hydrodynamical behavior of flow and heat transfer of water/CuO nanofluid in microchannel heat sink. They increased the heat transfer

Table 2 Changes of studied grid number in the present research

| Re	Parameters	Number of grid							
		20,000		50,000		70,000		95,000	
			Error%		Error%		Error%		Error%
$Re = 150$									
	Nu_{ave}	2.4532	23.68	3.0965	3.8	3.1813	1	3.2145	Base
	ΔP/pa	2.563e7	11	2.8312e7	5	2.8461e7	1	2.8463e7	Base
$Re = 700$									
	Nu_{ave}	4.957	15	5.4532	4.5	5.6755	0.45	5.7015	Base
	ΔP/pa	2.8754e7	0.8	2.8902e7	0.3	2.8951e7	0.14	2.8993e7	Base
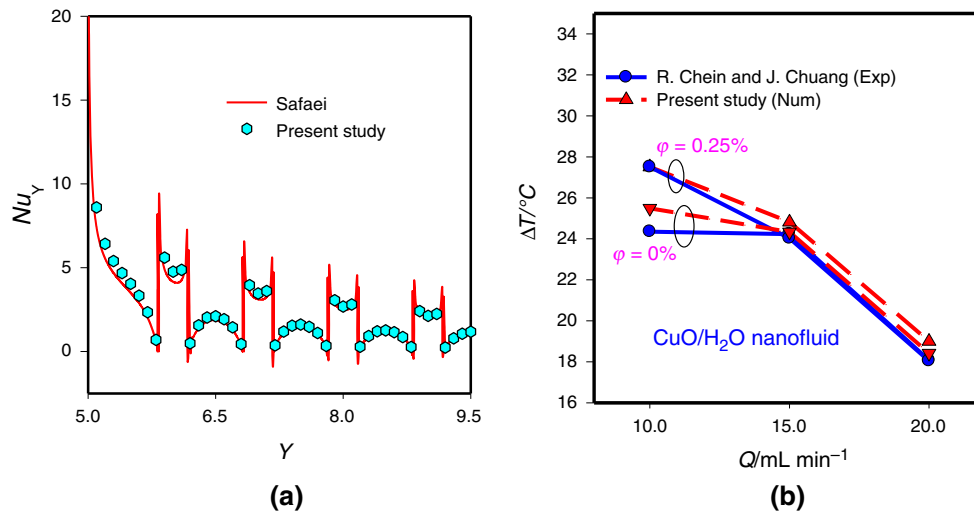
Fig. 3 Validation of present problem with the study of Safaei et al. [33] and Chein and Chuang [58]. **a** Numerical study, **b** experimental study

by using copper nanoparticles with volume fractions of 0–4% and different flow rates (Fig. 3b). According to Fig. 3, proper coincidence of present results with the studies of Safaei et al. [33] and Chein and Chuang [58] indicates that the present solving procedure and the applied boundary conditions are accurate.

Results and discussion

Figure 4 demonstrates the dimensionless temperature lines in Grashof numbers of 1000 and 10,000 and slip velocity coefficients of 0 and 0.1 for pure water fluid in Reynolds number of 100. Figure 4a investigates the effect of slip velocity coefficient on dimensionless temperature distribution inside the microchannel. It is observed that, by increasing slip velocity coefficient, cooling enhances on the solid wall. The reason of this behavior is because of non-zero velocity of fluid, which is in contact with solid wall in slip coefficient of 0.1. Figure 4b investigates the effect of Grashof number on temperature domain, and it is seen that, in hot areas of solid wall, the heat transfer improves considerably. Also, due to the enhancement of gravity domain and the influence of buoyancy force in Grashof number of 10,000, the cooling of these areas becomes considerable.

Figure 5 indicates the behavior of dimensionless temperature lines in different volume fractions and Grashof number of 1000 and slip velocity coefficient of 0 for pure water fluid in Reynolds number of 100. This figure studies the effect of using higher volume fractions on temperature distribution in different areas of microchannel. According to
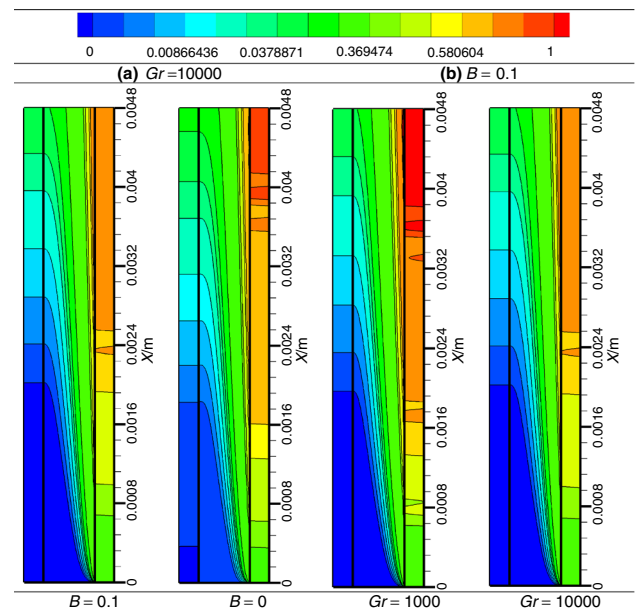
Fig. 4 Changes of dimensionless temperature lines in different Grashof numbers and slip velocity coefficients for pure water fluid in Reynolds number of 100. **a** $Gr = 10,000$, **b** $B = 0.1$

the contours of Fig. 5, by increasing volume fraction of nanoparticles, the heat transfer distribution inside the microchannel and especially on the solid walls becomes considerably uniform and temperature gradients reduce. The reason of this behavior is due to the augmentation of thermal conductivity coefficient of cooling fluid in contact with hot surfaces in higher volume fractions of nanoparticles. Also, by using pure water fluid, on the heated walls of
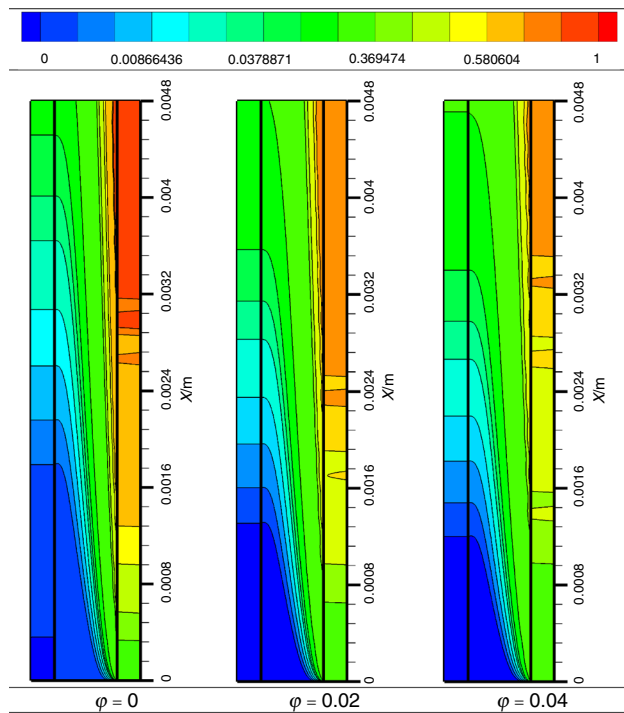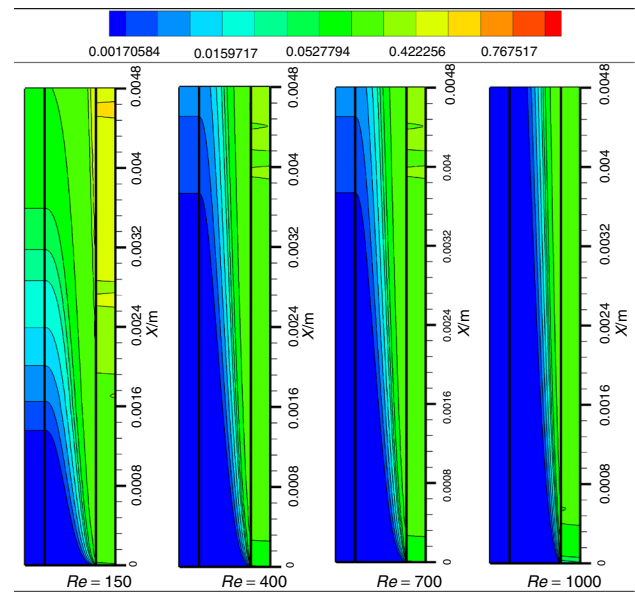
Fig. 5 Changes of dimensionless temperature lines in different volume fractions of nanoparticles and Grashof number of 1000

Fig. 6 Changes of dimensionless temperature lines in different Reynolds numbers

microchannel areas with lower heat transfer are created which are marked by red color, and these areas become more significant from the middle of microchannel to later on.

Figure 6 indicates the changes of dimensionless temperature lines in volume fraction of 4% of nanoparticles and Grashof number of 10,000 and slip velocity coefficient of 0.1 in different Reynolds numbers. In this study, the effect of Reynolds number changes on dimensionless temperature lines for the balanced values is investigated. By increasing fluid velocity, the convection heat transfer mechanism enhances significantly and the temperature distribution becomes uniform. By decreasing fluid velocity, because heat penetration to the upper layers of heated surface takes more time and fluid has sufficient time to be in contact with the heated surface, the non-uniform heat penetration to the upper layers of heated surface is completely obvious in Reynolds number of 150. By increasing fluid velocity, the dominancy of lower temperature of cooling fluid throughout the microchannel causes better distribution and the elimination of hot areas from microchannel walls.

In Fig. 7, the local friction coefficient on the heated wall for Reynolds numbers of 150 and 700 in Grashof numbers of 1000 and 10,000 with slip and no-slip boundary conditions on the solid walls is shown for investigating the effect of mentioned parameters and the enhancement of volume fraction of nanoparticles on the changes of local friction coefficient along the microchannel. According to Fig. 7a,

in lower velocities of fluid, because of more contact with solid walls, temperature gradients enhance causing the augmentation of shear stress and friction coefficient. Therefore, in all states, the level of Fig. 7a is higher than Fig. 7b. By increasing volume fraction of nanoparticles, due to the enhancement of nanoparticles collusion with the heated wall, fiction coefficient increases. Also, the slip velocity on solid walls does not prevent the fluid motion in these areas; hence, by increasing slip velocity coefficient, the friction coefficient reduces considerably. The increase in Grashof number causes significant changes in velocity gradients and consequently the augmentation of friction coefficient. According to the stated analogies and the relationship between the heat transfer enhancement and friction coefficient, in Fig. 7a and Grashof number of 10,000, the behavior of friction coefficient is affected by the oscillating heat transfer, and this behavior is not considerable in other figures. The reason is because of the great effect of buoyancy force (caused by oscillating heat transfer of heated surface) on fluid velocity parameters in Grashof number of 10,000 and Reynolds number of 150.

Figure 8 shows the behavior of local Nusselt number on the heated wall in Grashof number of 10,000 and slip velocity coefficient of 0.1 for Reynolds numbers of 400 and 1000. As it is seen, the behavior of local Nusselt number is affected by thermal boundary condition, and the changes of this parameter are oscillating. In all graphs of Fig. 8, by increasing volume fraction of nanoparticles and Reynolds number, the local Nusselt number improves. The maximum value of heat transfer accomplishes at the beginning of microchannel, and the reason is because of the maximum

Fig. 7 Local friction coefficient on the heated wall. **a** *Re* = 150, **b** *Re* = 700


(a)

(b)
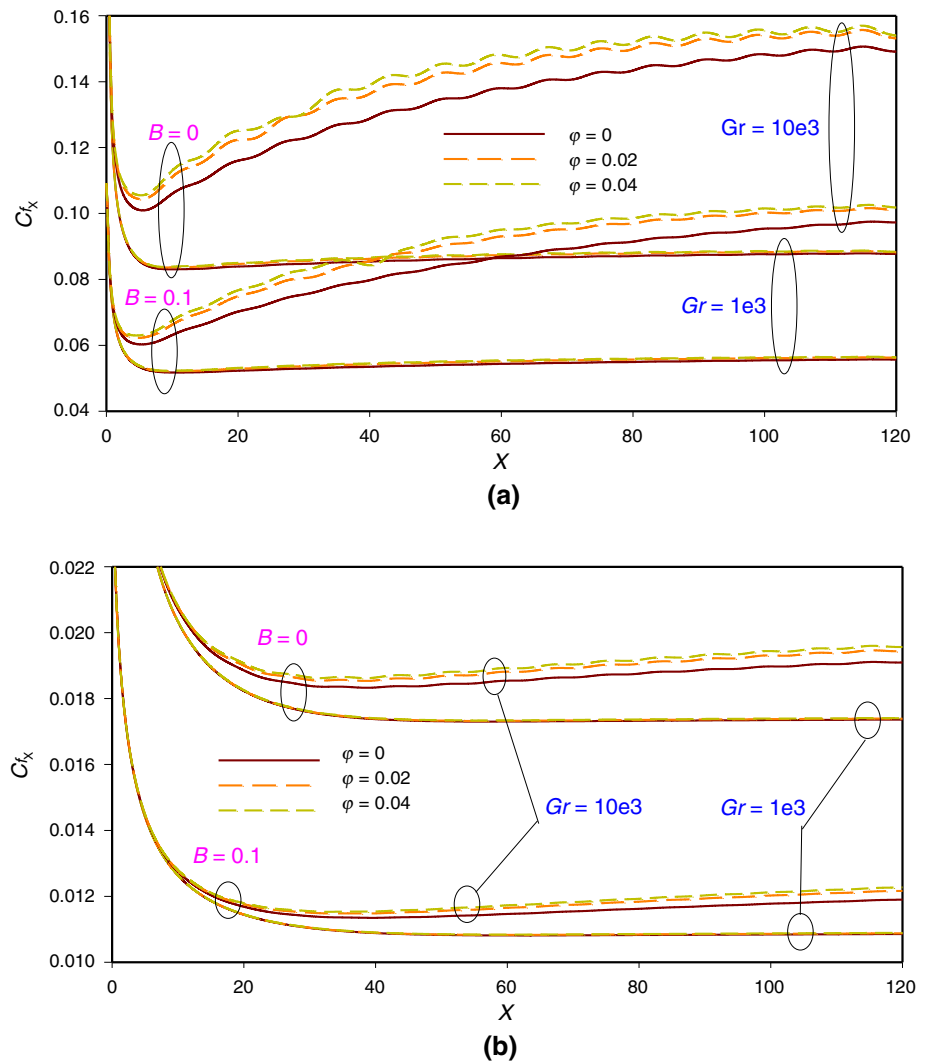
temperature differences of heated surface and fluid temperature in these areas. On the direction of fluid motion, the heat transfer intensity reduces gradually because of the enhancement and penetration of average temperature of fluid and the reduction of temperature difference of surface and fluid. According to the behavior of Fig. 8, in Reynolds number of 1000, the level of graphs is higher than Reynolds number of 400.

Figure 9 compares the values of average Nusselt number on the heated wall in different Grashof numbers, slip velocity coefficients and volume fractions. In all graphs, the maximum amount of heat transfer is related to Reynolds number of 1000 and volume fraction of 4% of solid nanoparticles and the slip velocity boundary condition on the solid wall and Grashof number of 10,000. By increasing volume fraction of nanoparticles, due to the improvement of thermal conductivity coefficient of cooling fluid and micron heat transfer mechanism of nanoparticles, heat transfer enhances. The existence of slip velocity on the solid walls

causes better heat transfer and the enhancement of convection heat transfer coefficient and Nusselt number and the reduction of temperature gradients. By increasing Grashof number, the buoyancy force along the fluid motion improves and the natural convection heat transfer becomes significant. Hence, in Grashof number of 10,000, graphs have higher levels. By increasing fluid velocity, the forced convection heat transfer enhances; therefore, Reynolds number of 1000 has the maximum value of heat transfer. It is observed that, in lower Reynolds numbers, the impressionability of heat transfer enhancement caused by Grashof number enhancement becomes more significant. Regarding this behavior, in constant B and in lower Reynolds numbers, graphs become divergent. Also, in higher Reynolds numbers, the importance of slip velocity on heat transfer enhancement caused by this boundary condition is more considerable. Therefore, by increasing Reynolds number and in constant φ, the average Nusselt number graphs become divergent.

Fig. 8 Local Nusselt number on the hated wall. **a** $Re = 400$, **b** $Re = 1000$

(a)

(b)

(a)

(b)

(c)
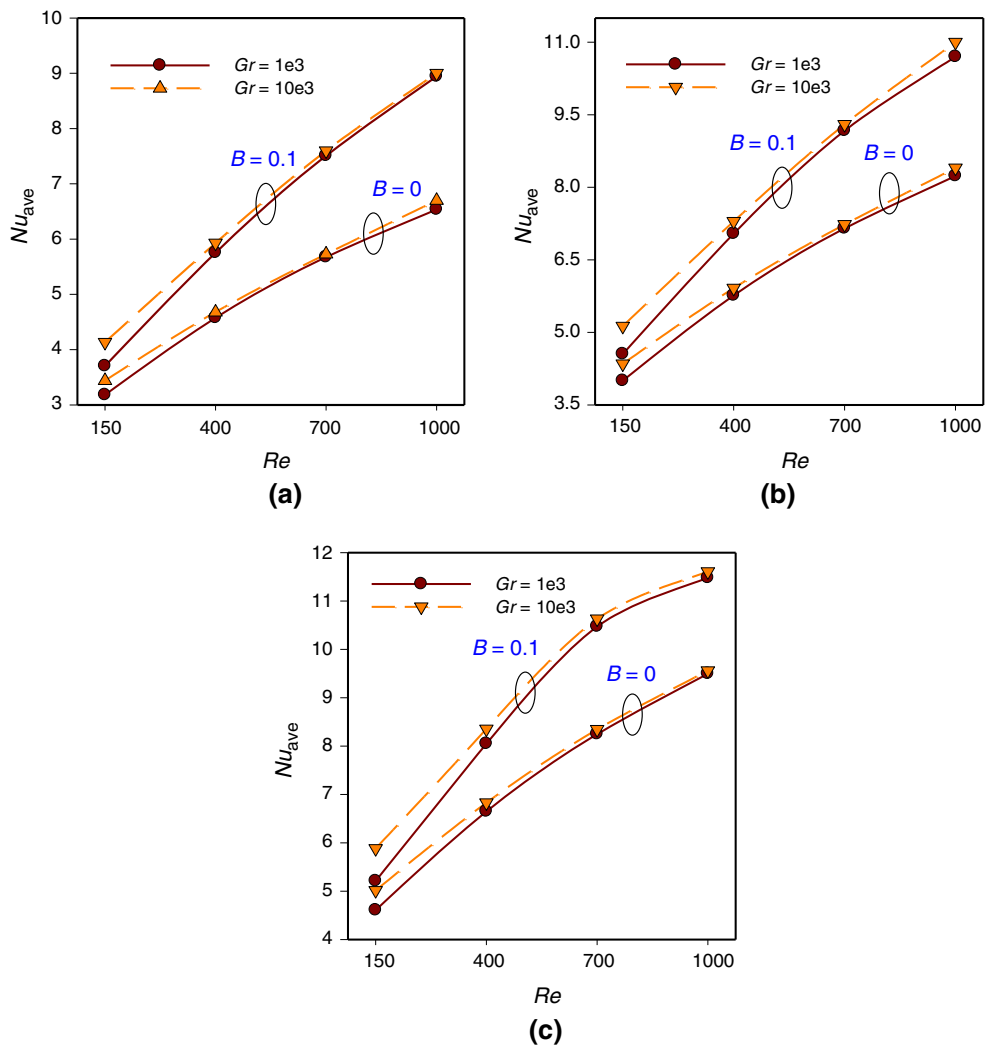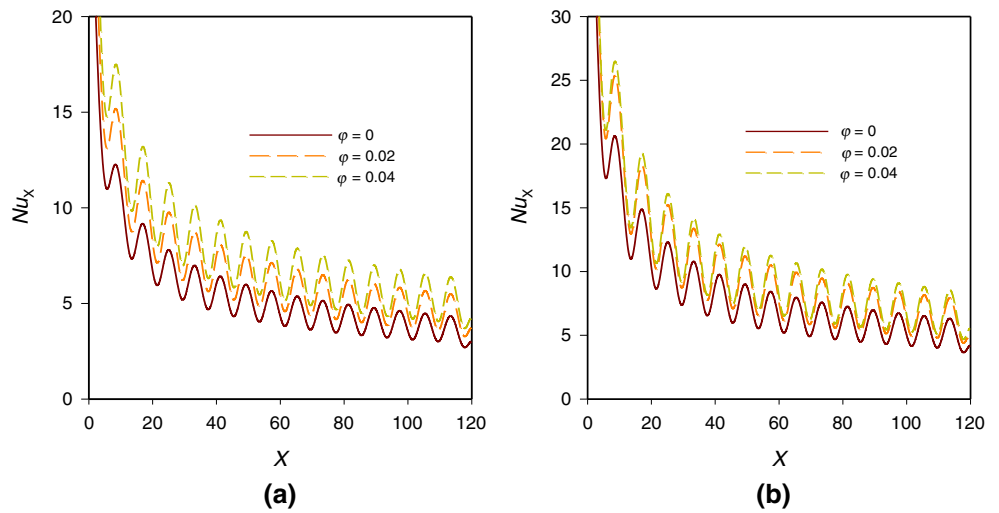
Fig. 9 Average Nusselt number on the heated wall. **a** $\varphi = 0$, **b** $\varphi = 0.02$, **c** $\varphi = 0.04$
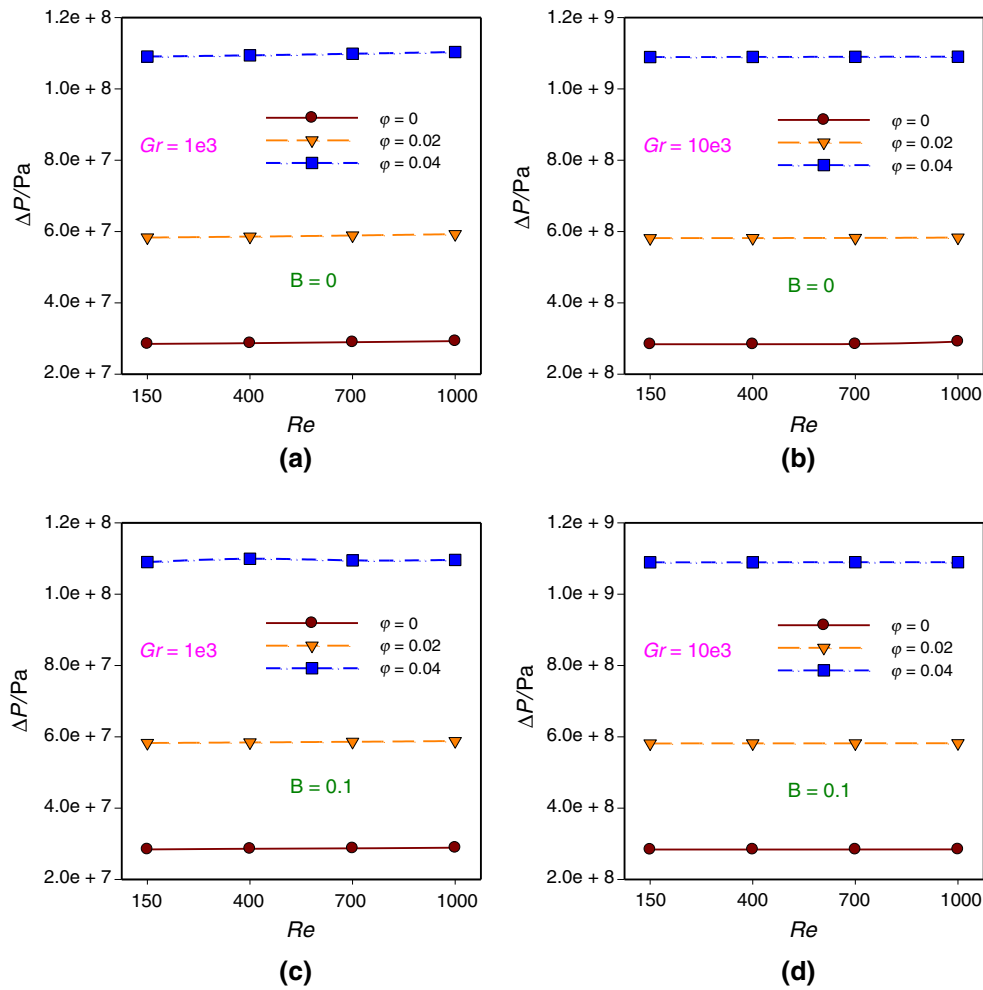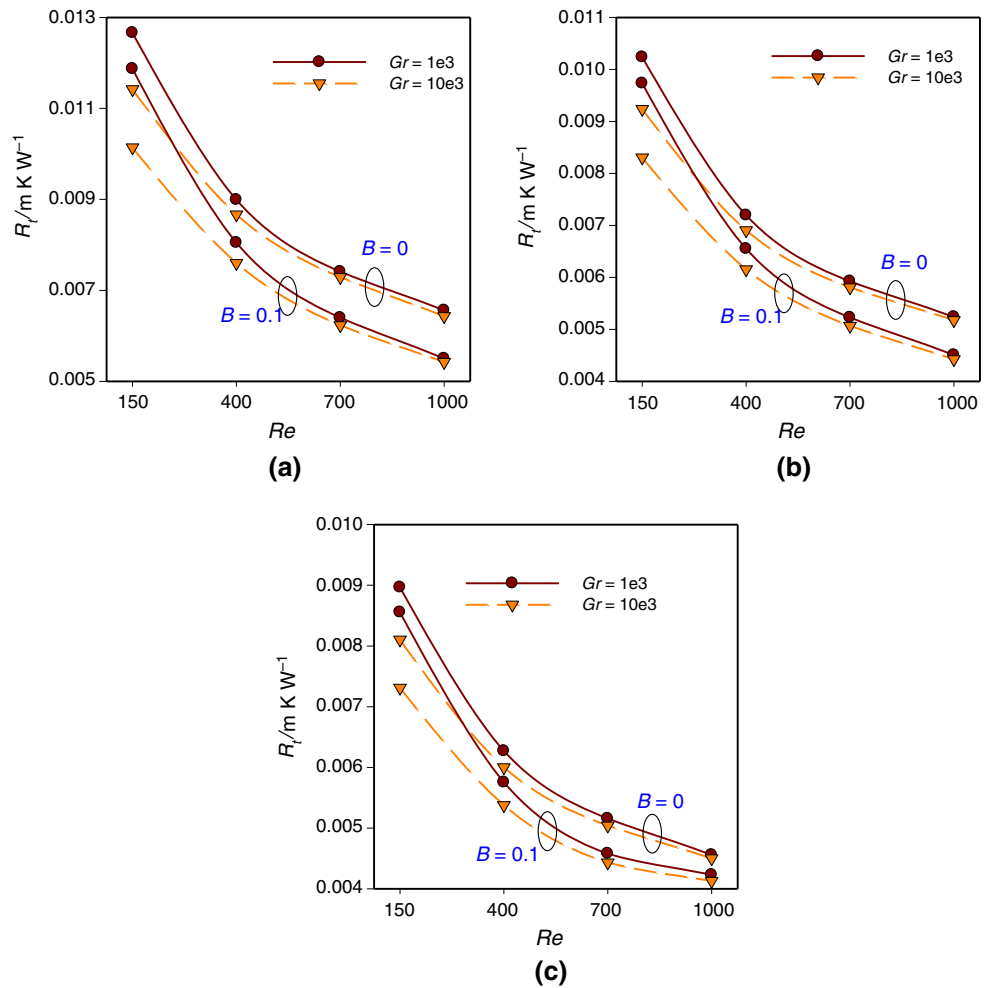
Fig. 10 Average pressure drop in different Reynolds numbers

Figure 10 indicates the changes of average pressure drop in different Grashof numbers, slip velocity coefficients, volume fractions of nanoparticles and Reynolds numbers. This figure investigates the effect of the enhancement of slip velocity and Grashof number on the changes of average pressure drop in different Reynolds numbers ranging from 150 to 1000. By increasing nanoparticles volume fraction, the density and viscosity of fluid are enhanced. Also, fluid with higher density has more momentum depreciation on its direction along the channel. On the other hand, fluid with higher viscosity has more contact with solid surfaces, and the transfer of velocity gradients among fluid layers happens with more pressure drop. By increasing slip velocity on the solid wall, due to the less prevention of solid surface on the direction of fluid motion and simple movement of fluid on walls, pressure drop reduces. Also, by increasing fluid velocity, due to the more momentum depreciation of fluid, pressure drop enhances.

Figure 11 demonstrates the behavior of average thermal resistance on the heated wall in Grashof numbers of 1000 and 100,000, slip velocity coefficients of 0 and 0.1 and volume fractions of 0–4%. This figure investigates the relationship between thermal resistance of heated surface with different slip velocity coefficients, Reynolds numbers, volume fractions of nanoparticles and Grashof numbers. According to this figure, by increasing Reynolds number, the buoyancy force, slip velocity coefficient on the solid wall, volume fraction and every factor causing the enhancement of heat transfer on the heated surfaces and the reduction of maximum temperature of surfaces entail the reduction thermal resistance of wall. By considering constant slip velocity coefficient, the ratio of thermal resistance to Grashof number reduces with the increase in Reynolds number. Therefore, by increasing Reynolds number, in constant B, the graphs of thermal resistance become convergent. Also, by increasing Grashof number

Fig. 11 Changes of average thermal resistance on the heated wall. **a** $\varphi = 0$, **b** $\varphi = 0.02$, **c** $\varphi = 0.04$

and slip velocity coefficient, the reduction of thermal resistance is significant in lower Reynolds numbers.

Figure 12 indicates the average entropy in different Grashof numbers, slip velocity coefficients and volume fractions of nanoparticles. The changes of entropy generation on flow direction are due to the entropy enhancement caused by heat transfer and friction coefficient. If fluid becomes irreversible on its direction, entropy generation enhances. According to the studied temperature contours and in Reynolds number of 150, the existence of hot areas on solid walls and on the top of the heated wall causes the augmentation of entropy generation. Also, because of the existence of no-slip boundary condition in collusion areas of fluid with wall, fluid velocity becomes 0. This behavior causes the increase in entropy generation caused by friction coefficient enhancement. The distribution of solid nanoparticles with higher volume fraction causes the reduction of temperature gradients and the dominancy of inlet cooling fluid temperature in most areas of microchannel. Therefore, the increase in volume fraction of

nanoparticles, slip velocity coefficient, Reynolds number and Grashof number cause the reduction of entropy.

Figure 13 shows the changes of local dimensionless temperature on the central line of flow in Grashof number of 1000 with the existence of no-slip boundary condition on solid walls. By entering the cooling fluid to microchannel, because of the existence of hated wall, temperature gradients grow gradually and the penetration of thermal boundary layer to the central core of flow becomes observable. The penetration of thermal boundary layer starts in Reynolds number of 150 in $X = 10$, and before this area, the inlet fluid temperature becomes dominated in central line of flow. By increasing Reynolds number, the heat penetration to the central core of flow postpones and in Reynolds number of 700 starts in $X = 40$. In fact, this postponement and the dominancy of cooling fluid temperature on channel entail heat transfer enhancement with the augmentation of Reynolds number. Also, the increase in volume fraction of nanoparticles causes the enhancement of dimensionless temperature in central line of flow.
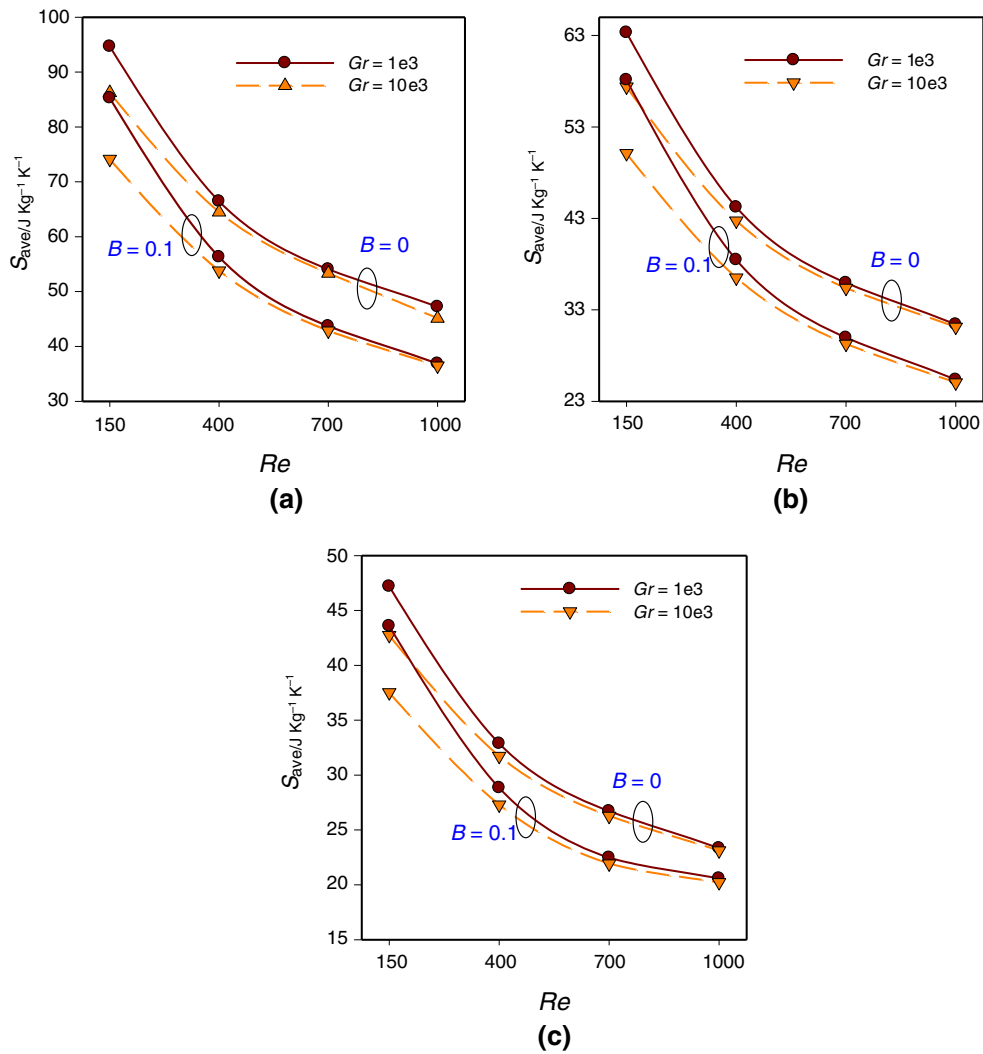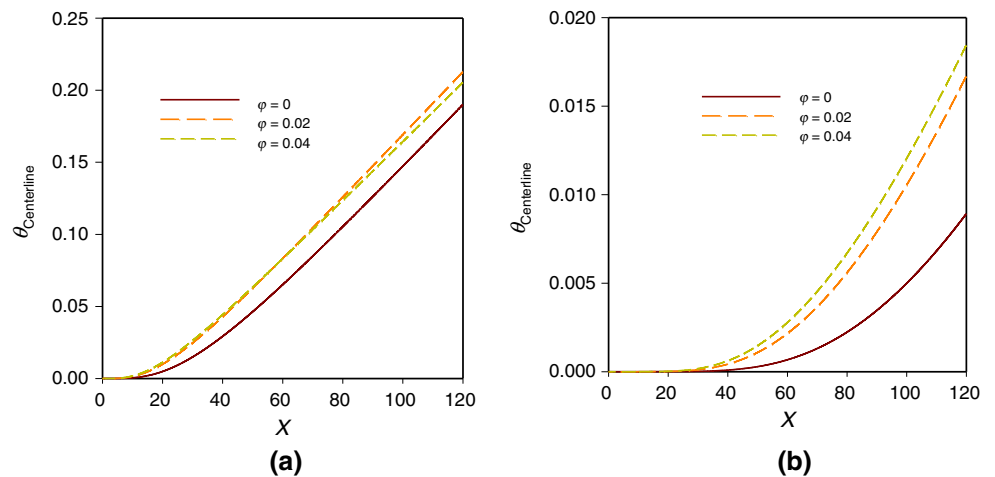
Fig. 12 Behavior of entropy generation on the solid wall. **a** $\varphi = 0$, **b** $\varphi = 0.02$, **c** $\varphi = 0.04$

Fig. 13 Distribution of dimensionless temperature in the central line of flow. **a** Re = 150, **b** Re = 700

Conclusions

In the present paper, the effect of using water/Ag nanofluid with 0–4% nanoparticles volume fractions with slip and no-slip boundary conditions on the solid walls of a two-dimensional rectangular microchannel with Reynolds numbers of 150–1000 has been investigated by applying gravity acceleration domain in Grashof numbers of 1000 and 10,000 using finite volume method in Cartesian coordinates. The obtained results indicate that, in vertical microchannel, the heat transfer enhancement depends on boundary condition, velocity domain and gravity acceleration. Also, the changes of local friction coefficient profile in low fluid velocities (Reynolds number of 150) and Grashof number of 10,000 depend on temperature profile. According to the average Nusselt number figures, in low Reynolds numbers, the increase in this parameter caused by Grashof number augmentation is more significant. Based on this behavior, in constant slip velocity coefficient and low Reynolds numbers, the figures become divergent. Also, in higher Reynolds numbers, the importance of slip velocity boundary condition on heat transfer enhancement becomes more considerable. Therefore, by increasing Reynolds number, the average Nusselt number figures in constant volume fraction of nanoparticles become divergent. The enhancement of Reynolds number, slip velocity coefficient, Grashof number and volume fraction of nanoparticles entail the augmentation of Nusselt number and the reduction of thermal resistance.

References

1. Siavashi M, Jamali M. Heat transfer and entropy generation analysis of turbulent flow of TiO$_2$–water nanofluid inside annuli with different radius ratios using two-phase mixture model. Appl Therm Eng. 2016;100:1149–60.
2. Yousofvand R, Derakhshan Sh, Ghasemi K, Siavashi M. MHD transverse mixed convection and entropy generation study of electromagnetic pump including a nanofluid using 3D LBM simulation. Int J Mech Sci. 2017. https://doi.org/10.1016/j.ijmecsci.2017.08.034.
3. Ghasemi K, Siavashi M. MHD nanofluid free convection and entropy generation in porous enclosures with different conductivity ratios. J Magn Magn Mater. 2017. https://doi.org/10.1016/j.jmmm.2017.07.028.
4. Barzegarian R, Aloueyan A, Yousefi T. Thermal performance augmentation using water based Al$_2$O$_3$–gamma nanofluid in a horizontal shell and tube heat exchanger under forced circulation. Int Commun Heat Mass Transf. 2017;86:52–9.
5. Siavashi M, Talesh Bahrami HR, Saffari H. Numerical investigation of flow characteristics, heat transfer and entropy generation of nanofluid flow inside an annular pipe partially or completely filled with porous media using two-phase mixture model. Energy. 2015;93:2451–66.
6. Rashidi S, Mahian O, Mohseni Languri E. Applications of nanofluids in condensing and evaporating systems. J Therm Anal Calorim. 2017. https://doi.org/10.1007/s10973-017-6773-7.
7. Siavashi M, Talesh Bahrami HR, Saffari H. Numerical investigation of porous rib arrangement on heat transfer and entropy generation of nanofluid flow in an annulus using a two-phase mixture model. Numer Heat Transf Part A Appl. 2017. https://doi.org/10.1080/10407782.2017.1345270.
8. Rashidi S, Eskandarian M, Mahian O, Poncet S. Combination of nanofluid and inserts for heat transfer enhancement. J Therm Anal Calorim. 2018. https://doi.org/10.1007/s10973-018-7070-9.
9. Siavashi M, Rostami A. Two-phase simulation of non-Newtonian nanofluid natural convection in a circular annulus partially or completely filled with porous media. Int J Mech Sci. 2017;133:689–703.
10. Darbari B, Rashidi S, Abolfazli Esfahani J. Sensitivity analysis of entropy generation in nanofluid flow inside a channel by response surface methodology. Entropy. 2016;18:1–16.
11. Javadi P, Rashidi S, Abolfazli Esfahani J. Flow and heat management around obstacle by nanofluid and incidence angle. J Thermophys Heat Transf. 2017;31:983–8.
12. Barzegarian R, Moraveji MK, Aloueyan A. Experimental investigation on heat transfer characteristics and pressure drop of BPHE (brazed plate heat exchanger) using TiO$_2$–water nanofluid. Exp Therm Fluid Sci. 2016;74:11–8.
13. Siavashi M, Jamali M. Optimal selection of annulus radius ratio to enhance heat transfer with minimum entropy generation in developing laminar forced convection of water–Al$_2$O$_3$ nanofluid flow. J Cent South Univ. 2017;24:1850–65.
14. Ghasemi K, Siavashi M. Lattice Boltzmann numerical simulation and entropy generation analysis of natural convection of nanofluid in a porous cavity with different linear temperature distributions on side walls. J Mol Liq. 2017;233:415–30.
15. Keshavarz Moraveji M, Barzegarian R, Bahiraei M, Barzegarian M, Aloueyan A, Wongwises S. Numerical evaluation on thermal-hydraulic characteristics of dilute heat-dissipating nanofluids flow in microchannels. J Therm Anal Calorim. 2018. https://doi.org/10.1007/s10973-018-7181-3.
16. Zeibi Shirejini S, Rashidi S, Esfahani JA. Recovery of drop in heat transfer rate for a rotating system by nanofluids. J Mol Liq. 2016;220:961–9.
17. Yaghoubi Emami R, Siavashi M, Shahriari Moghaddam Gh. The effect of inclination angle and hot wall configuration on Cu–water nanofluid natural convection inside a porous square cavity. Adv Powder Technol. 2018. https://doi.org/10.1016/j.apt.2017.10.027.
18. Siavashi M, Yousofvand R, Rezanejad S. Nanofluid and porous fins effect on natural convection and entropy generation of flow inside a cavity. Adv Powder Technol. 2017. https://doi.org/10.1016/j.apt.2017.10.021.
19. Goshayeshi HR, Goodarzi M, Dahari M. Effect of magnetic field on the heat transfer rate of kerosene/Fe$_2$O$_3$ nanofluid in a copper oscillating heat pipe. Exp Therm Fluid Sci. 2015;68:663–8.
20. Akbarzadeh M, Rashidi S, Karimi N, Omar N. First and second laws of thermodynamics analysis of nanofluid flow inside a heat exchanger duct with wavy walls and a porous insert. J Therm Anal Calorim. 2018. https://doi.org/10.1007/s10973-018-7044-y.
21. Goodarzi M, Kherbeet ASh, Afrand M, Sadeghinezhad E, Mehrali M, Zahedi P, Wongwises S, Dahari M. Investigation of heat transfer performance and friction factor of a counter-flow double-pipe heat exchanger using nitrogen-doped, graphene-based nanofluids. Int Commun Heat Mass Transf. 2016;76:16–23.
22. Goshayeshi HR, Goodarzi M, Safaei MR, Dahari M. Experimental study on the effect of inclination angle on heat transfer enhancement of a ferro-nanofluid in a closed loop oscillating heat pipe under magnetic field. Exp Therm Fluid Sci. 2016;74:265–70.

23. Akar Sh, Rashidi S, Esfahani JA. Second law of thermodynamic analysis for nanofluid turbulent flow around a rotating cylinder. J Therm Anal Calorim. 2017. https://doi.org/10.1007/s10973-017-6907-y.

24. Rashidi S, Akbarzadeh M, Karimi N, Masoodi R. Combined effects of nanofluid and transverse twisted-baffles on the flow structures, heat transfer and irreversibilities inside a square duct—a numerical study. Appl Therm Eng. 2018;130:135–48.

25. Parizad R, Rashidi S, Esfahani JA. Experimental investigation of nanofluid free convection over the vertical and horizontal flat plates with uniform heat flux by PIV. Adv Powder Technol. 2016;27:312–22.

26. Esfahani JA, Safaei MR, Goharimanesh M, Oliveira LRD, Goodarzi M, Shamshirband Sh, Filho EPB. Comparison of experimental data, modelling and non-linear regression on transport properties of mineral oil based nanofluids. Powder Technol. 2017;317:458–70.

27. Rashidi S, Javadi P, Esfahani JA. Second law of thermodynamics analysis for nanofluid turbulent flow inside a solar heater with the ribbed absorber plate. J Therm Anal Calorim. 2018. https://doi.org/10.1007/s10973-018-7164-4.

28. Rashidi S, Esfahani JA. Optimum interaction between magnetohydrodynamics and nanofluid for thermal and drag management. J Thermophys Heat Transf. 2017;31:218–29.

29. Safaei MR, Ahmadi G, Goodarzi MSh, Safdari Shadloo M, Goshayeshi HR, Dahari M. Heat transfer and pressure drop in fully developed turbulent flow of graphene nanoplatelets–silver/water nanofluids. Fluids. 2016;1(3):1–20.

30. Safaei MR, Ahmadi G, Goodarzi MSh, Kamyar A, Kazi SN. Boundary layer flow and heat transfer of FMWCNT/water nanofluids over a flat plate. Fluids. 2016;1(4):1–13.

31. Goshayeshi HR, Safaei MR, Goodarzi M, Dahari M. Particle size and type effects on heat transfer enhancement of ferro-nanofluids in a pulsating heat pipe under magnetic field. Powder Technol. 2016;301:1218–26.

32. Nikkhah Z, Karimipour A, Safaei MR, Forghani-Tehrani P, Goodarzi M, Dahari M, Wongwises S. Forced convective heat transfer of water/functionalized multi-walled carbon nanotube nanofluids in a microchannel with oscillating heat flux and slip boundary condition. Int Commun Heat Mass Transf. 2015;68:69–77.

33. Safaei MR, Gooarzi M, Akbari OA, Safdari Shadloo M and Dahari M. Performance evaluation of nanofluids in an inclined ribbed microchannel for electronic cooling applications, "electronics cooling", Prof. S M Sohel Murshed (ed.), InTech; 2016. https://doi.org/10.5772/62898. http://www.intechopen.com/books/electronics-cooling/performance-evaluation-of-nanofluids-in-an-inclined-ribbed-microchannel-for-electronic-cooling-appli.

34. Raisi A, Ghasemi B, Aminossadati SM. A numerical study on the forced convection of laminar nanofluid in a microchannel with both slip and no slip condition. Numer Heat Transf A Appl. 2011;59:114–29.

35. Elshazly K, Moawed M, Ibrahim E, Emara M. Heat transfer by free convection from the inside surface of the vertical and inclined elliptic tube. Energy Convers Manag. 2005;46:1443–63.

36. Lotfi R, Saboohi Y, Rashidi AM. Numerical study of forced convection heat transfer of nanofluids: comparison of different approaches. Int Commun Heat Mass Transf. 2010;37:74–8.

37. Behzadmehr A, Saffar-Avval M, Galanis N. Prediction of turbulent forced convection of a nanofluid in a tube with uniform heat flux using two phase approach. Int J Heat Fluid Flow. 2007;28:211–9.

38. Akbari OA, Karimipour A, Toghraie Semiromi D, Safaei MR, Alipour H, Goodarzi M, Dahari M. Investigation of Rib's height effect on heat transfer and flow parameters of laminar water–

39. Behnampour A, Akbari OA, Safaei MR, Ghavami M, Marzban A, Ahmadi Sheikh Shabani Gh, Zarringhalam M, Mashayekhi R. Analysis of heat transfer and nanofluid fluid flow in microchannels with trapezoidal, rectangular and triangular shaped ribs. Physica E. 2017;91:15–31.

40. Karimipour A, Alipour H, Akbari OA, Toghraie Semiromi D, Esfe MH. Studying the effect of indentation on flow parameters and slow heat transfer of water–silver nanofluid with varying volume fraction in a rectangular two-dimensional microchannel. Indian J Sci Technol. 2015;8(15):51707.

41. Siavashi M, Talesh Bahrami HR, Aminian E. Optimization of heat transfer enhancement and pumping power of a heat exchanger tube using gradient and multi-layered porous foams. Appl Therm Eng. 2018. https://doi.org/10.1016/j.applthermaleng.2018.04.066.

42. Toosi MH, Siavashi M. Two-phase mixture numerical simulation of natural convection of nanofluid flow in a cavity partially filled with porous media to enhance heat transfer. J Mol Liq. 2017. https://doi.org/10.1016/j.molliq.2017.05.015.

43. Alikhani S, Behzadmehr A, Saffar-Avval M. Numerical study of nanofluid mixed convection in a horizontal curved tube using two-phase approach. Heat Mass Transf. 2011;47:107–18.

44. Gravndyan Q, Akbari OA, Toghraie D, Marzban A, Mashayekhi R, Karimi R, Pourfattah F. The effect of aspect ratios of rib on the heat transfer and laminar water/TiO$_2$ nanofluid flow in a two-dimensional rectangular microchannel. J Mol Liq. 2017;236:254–65.

45. Chon H, Kihm KD, Lee SP, Choi SUS. Empirical correlation finding the role of temperature and particle size for nanofluid (Al$_2$O$_3$) thermal conductivity enhancement. Appl Phys Lett. 2005;87:1–3.

46. Alipour H, Karimipour A, Safaei MR, Toghraie Semiromi D, Akbari OA. Influence of T-semi attached rib on turbulent flow and heat transfer parameters of a silver–water nanofluid with different volume fractions in a three-dimensional trapezoidal microchannel. Physica E. 2017;88:60–76.

47. Maiga SE, Nguyen CT, Galanis N, Roy G. Heat transfer behaviors of nanofluids in a uniformly heated tube. Super Lattices Microstruct. 2004;35:543–57.

48. Turkyilmazoglu M. Performance of direct absorption solar collector with nanofluid mixture. Energy Convers Manag. 2016;114:1–10.

49. Khanafer K, Vafai K, Lightstone M. Buoyancy-driven heat transfer enhancement in a two dimensional enclosure utilizing nanofluids. Int J Heat Mass Transf. 2003;46:3639–53.

50. Akbari OA, Goodarzi M, Safaei MR, Zarringhalam M, Ahmadi Sheikh Shabani GhR, Dahari M. A modified two-phase mixture model of nanofluid flow and heat transfer in 3-D curved microtube. Adv Powder Technol. 2016;27:2175–85.

51. Akbari OA, Toghraie D, Karimipour A, Marzban A, Ahmadi GR. The effect of velocity and dimension of solid nanoparticles on heat transfer in non-Newtonian nanofluid. Physica E. 2017;86:68–75.

52. Shamsi MR, Akbari OA, Marzban A, Toghraie D, Mashayekhi R. Increasing heat transfer of non-Newtonian nanofluid in rectangular microchannel with triangular ribs. Physica E. 2017;93:167–78.

53. Leng C, Wang XD, Wang TH, Yan WM. Multi-parameter optimization of flow and heat transfer for a novel double-layered microchannel heat sink. Int J Heat Mass Transf. 2015;84:359–69.

54. Bejan A. Entropy Generation through heat and fluid flow. New York: Wiley; 1982.

55. Mahian O, Kianifar A, Kleinstreuer C, Al-Nimr MA, Pop I, Sahin AZ, Wongwises S. A review of entropy generation in nanofluid flow. Int J Heat Mass Transf. 2013;65:514–32.

56. Rezaei O, Akbari OA, Marzban A, Toghraie D, Pourfattah F, Mashayekhi R. The numerical investigation of heat transfer and pressure drop of turbulent flow in a triangular microchannel. Physica E. 2017;93:179–89.

57. Abbasian Arani AA, Akbari OA, Safaei MR, Marzban A, Alrashed AAAA, Ahmadi GhR, Nguyen TK. Heat transfer improvement of water/single-wall carbon nanotubes (SWCNT) nanofluid in a novel design of a truncated double layered microchannel heat sink. Int J Heat Mass Transf. 2017;113:780–95.

58. Chein R, Chuang J. Experimental microchannel heat sink performance studies using nanofluids. Int J Therm Sci. 2007;46:57–66.